Basal neural stem cells in the subventricular zone drive postnatal neurogenesis with apical stem cells acting as proliferation gate-keepers

Katja Baur[1*], Yomn Abdullah[1, 2*], Claudia Mandl[1], Gabriele Hölzl-Wenig[1], Yan Shi[1,3], Udo Edelkraut[1,4], Priti Khatri[1,5], Francesca Ciccolini[1].
*equal contribution.

[1]Department of Neurobiology, Interdisciplinary Center for Neurosciences, University of Heidelberg, Heidelberg, Germany.
[2]Current address: Division of Systems Biology of Signal Transduction, German Cancer Research Center (DKFZ), Heidelberg, Germany
[3]Current address: Department of Human Genetics, Radboud University Medical Center, Nijmegen, The Netherlands.
[4]Current address: Molecular Health GmbH, Heidelberg, Germany
[5]Current address: ICGC lab, Advanced Centre for Treatment, Research and Education in Cancer, Tata Memorial Centre, Navi Mumbai, India

Correspondence should be addressed to:
Dr Francesca Ciccolini; Email: Ciccolini@nbio.uni-heidelberg.de
Department of Neurobiology, Interdisciplinary Center for Neurosciences (IZN), University of Heidelberg, Im Neuenheimer Feld 366, 69120 Heidelberg, Germany
Phone: +49-6221-548696 Fax: +49-6221-546700

Running title: Basal Neural stem cells in the V-SVZ.
Keywords: Neural stem cells, Tlx, Notch signaling, neurogenesis, Subventricular Zone.

Graphical Abstract

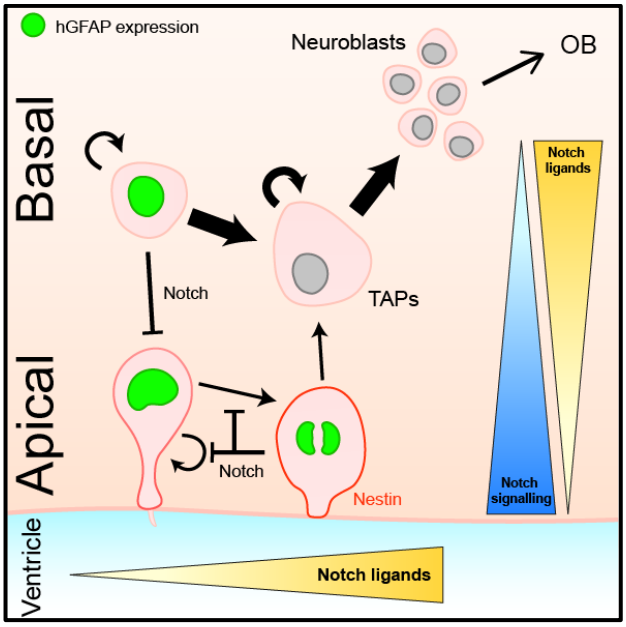

Highlights

- Basal NSCs are the most abundant stem cell type in the adult V-SVZ from birth onwards.
- Apical and basal NSCs display distinct characteristics and cell cycle progression dynamics.
- Apical NSCs are not the main source of newly generated adult OB interneurons.
- Apical NSCs regulate intermediate progenitor proliferation by orchestrating Notch-mediated lateral inhibition.

Abstract

Neural stem cells (NSCs) in the ventricular-subventricular zone (V-SVZ) contribute to olfaction by being the origin of most adult-born olfactory bulb (OB) interneurons. The current consensus maintains that adult NSCs are radial glia-like progenitors apically contacting the lateral ventricle and generating intermediate progenitors migrating at the basal V-SVZ. Whether basal NSCs are present in the V-SVZ is unknown. We here used genetic tagging of NSCs *in vivo* and additional labelling approaches to reveal that basal NSCs lacking apical attachment represent the largest NSC type in the postnatal V-SVZ from birth onwards. Despite dividing faster than their apical counterpart, basal NSCs still undergo long-term self-renewal and quiescence. Unlike apical NSCs, they are largely devoid of primary cilia and Prominin-1, Nestin and glial fibrillary acidic protein (GFAP) immunoreactivity. Six weeks after viral tagging of apical cells, few descendant cells were detected in the basal V-SVZ, including Sox9$^+$ progenitors and GFAP$^+$ astrocytes, and very rare new neurons in the OB, indicating that adult-born OB neurons originate from basal and not apical NSCs. Consistent with this, we found that pregnancy, a physiological modulator of adult OB neurogenesis, selectively increases the number of basal but not apical NSCs. Lastly, we find that apical NSCs display the highest levels of Notch activation in the neural lineage, and that selective apical downregulation of Notch-signaling effector Hes1 decreases Notch activation while increasing proliferation across the V-SVZ. Thus, apical NSCs act essentially as neurogenesis gatekeepers by modulating Notch-mediated lateral inhibition of proliferation in the adult V-SVZ.

Introduction

The adult mammalian brain, despite showing a general inability to repair and regenerate, encompasses neural stem cells (NSCs) which are capable of self-renewing and generating more differentiated cells upon cell division (Gage 2002; Obernier and Alvarez-Buylla 2019). First evidence of proliferation and neurogenesis in the adult rodent brain was reported more than fifty years ago (Altman 1962; Altman and Das 1965). Since then, researchers have focused on investigating adult neurogenesis and the cell types contributing to this process. In mice, NSCs were originally retrospectively identified by means of clonal assays, demonstrating that the epidermal growth factor (EGF) elicits the proliferation of rare self-renewing and multipotent adult brain cells (Reynolds and Weiss 1992). Thereafter, it was shown that neurogenesis continues throughout adulthood in the dentate gyrus and in the olfactory bulb (OB) driven by NSCs residing in the subgranular zone (SGZ) of the hippocampus and in the ventricular-subventricular zone (V-SVZ) lining the lateral ventricles, respectively (reviewed in Ming and Song 2011). In rodents, the largest neurogenic niche is the V-SVZ, where adult-born neuroblasts migrate along the rostral migratory stream to the OB where they differentiate into GABAergic and, to a lesser extent, glutamatergic interneurons (Lois, Garcia-Verdugo, and Alvarez-Buylla 1996; Merkle,

Mirzadeh, and Alvarez-Buylla 2007; Brill et al. 2009). This process of neurogenesis in mice contributes to odor recognition (reviewed in Feierstein 2012) and is modulated by conditions engaging the olfactory function like the behaviour associated with mating and parental bonding (Shingo et al. 2003; Furuta and Bridges 2005).

Most neural cells in the adult murine brain originate from radial glia progenitors (Malatesta et al. 2003; Anthony et al. 2004). Radial glia cells are first generated at the onset of neurogenesis between embryonic day (E) 10 and 12 (Kriegstein and Gotz 2003), and display an apical-basal polarity with an apically located centrosome. During brain development, apical radial glia give rise to so-called basal radial glia progenitors, which lack apical attachment, undergo mitosis at the basal side of the niche and are critical for the numeric expansion of neurons, which distinguishes gyrencephalic brains (Florio and Huttner 2014; Penisson et al. 2019). Throughout development, apical radial glia cells express Nestin (Hockfield and McKay 1985) and Prominin-1 (Weigmann et al. 1997), however, during the first postnatal week, they acquire expression of the astroglial marker glial fibrillary acidic protein (GFAP) and begin to lose Nestin expression in most brain regions (Misson et al. 1991; Kalman and Pritz 2001; Alves et al. 2002). Adult NSCs are generated from radial glia (Merkle, Mirzadeh, and Alvarez-Buylla 2007; Ortiz-Alvarez et al. 2019) and a large portion of NSCs in the adult V-SVZ are selected during mid to late development when a subset of embryonic radial glia enters quiescence (Fuentealba et al. 2015; Furutachi et al. 2015; Hu et al. 2017; Yuzwa et al. 2017). Previous studies have highlighted the presence of radial glia-like cells in the adult apical V-SVZ and have shown their NSC characteristics by demonstrating their neurogenic and regenerative potential (Doetsch et al. 1999; Doetsch, Garcia-Verdugo, and Alvarez-Buylla 1999). These radial glia-like NSCs are characterized by apical-basal polarity, extending a long basal process to the blood vessels and a primary cilium into the lateral ventricle (Mirzadeh et al. 2008; Shen et al. 2008; Tavazoie et al. 2008). Despite showing a certain degree of heterogeneity, which reflects changes in cell cycle, most apical NSCs express Nestin, GFAP, Prominin-1 and high levels of epidermal growth factor receptor (EGFR) during proliferation (Doetsch et al. 1999; Khatri et al. 2014; Codega et al. 2014). High levels of EGFR expression are maintained in more differentiated intermediate progenitors, including transit amplifying progenitors (Type C cells; TAPs) and pre-neuroblasts, which downregulate EGFR expression during neuronal differentiation (Cesetti et al. 2009; Carrillo-Garcia et al. 2010). Whereas gene tagging has shown that GFAP and Prominin-1 expressing NSCs contribute to neurogenesis in the olfactory bulb (OB) (Doetsch et al. 1999; Garcia et al. 2004; Beckervordersandforth et al. 2010; Weber et al. 2011), it is unclear whether these tagged cells all represent apical radial glia-like NSCs. Indeed, several lines of evidence point to the possibility that an additional pool of NSCs, lacking an apical contact with the lateral ventricles, is present at the basal side of the V-SVZ. For example, during the first week after birth most apical radial glia cells in the V-SVZ lose apical attachment and accumulate at the basal side of the SVZ undergoing complex morphological changes (Alves et al. 2002; Tramontin et al. 2003). Moreover, at later postnatal ages, proliferating astrocytes, i.e. type B2 cells, which lack an apical attachment, are also present in the adult V-SVZ (Doetsch, Garcia-Verdugo, and Alvarez-Buylla 1997) and with increasing postnatal age, apical NSCs lose apical

attachment and migrate to the basal V-SVZ, where they proliferate and further differentiate (Obernier et al. 2018). However, it is unknown whether these basal progenitors represent NSCs and if they contribute to OB adult neurogenesis.
We here show the presence of basal progenitor cells which display NSC characteristics as well as undergo long-term quiescence and self-renewal in the adult V-SVZ. We found that basal NSCs are the largest NSC pool in the postnatal V-SVZ from birth onwards and the main source of adult-born OB interneurons. Moreover, we observed that pregnancy, which leads to an expansion of the NSC pool in the V-SVZ (Shingo et al. 2003), selectively increases their number, showing that the generation of basal NSCs is a process autonomous from apical NSC consumption.

Methods

Animals and SVZ dissection
All animal experiments were approved by the Regierungspräsidium Karlsruhe and the local authorities of Heidelberg University. C57BL/6 (Wildtype, WT) and hGFAP-tTA;H2B-GFP (hGFAP;H2B-GFP) mice were sacrificed by CO_2 inhalation followed by cervical dislocation (adult), or by decapitation (neonatal). For DiI analyses, brains were placed on a petri dish, the V-SVZ apical surface was exposed and DiI (1,1'-Dioctadecyl-3,3,3',3'-Tetramethylindocarbocyanine Perchlorate, ThermoFisher Scientific) was applied for 1 minute followed by washing in sort medium (Luque-Molina et al. 2019). For the analysis of the effect of pregnancy, pregnant dams were sacrificed two weeks after having given birth. Littermate virgin controls were sacrificed at the same time.

Fluorescence activated cell sorting (FACS)
V-SVZ cells were dissociated and incubated at 4°C in sort medium containing anti-Prominin1-APC antibody or Anti-Prominin-1-PE for 30 min. For experiments requiring EGFR labelling, cells were incubated for further 30 min with recombinant human EGF conjugated to Alexa Fluor 488 or Alexa Fluor 647. Thereafter, cells were rinsed twice in sort medium before being stained with Propidium Iodide (PI, 1:100) to eliminate dead cells and sorted with a FACSAria II flow cytometer (BD Biosciences, Heidelberg, Germany) like previously described (Cesetti et al. 2009; Ciccolini et al. 2005; Khatri et al. 2014). For clonal analysis, FACS sorted neural stem cells were plated for neurosphere cultures as previously explained (Ciccolini et al. 2005).
For the analysis of self-renewal *in vivo*, we calculated the percentage of H2B-GFP expressing (G^+) cells displaying high or intermediate levels of fluorescence as described before (Luque-Molina et al. 2017). Briefly, H2B-GFP fluorescence levels were plotted on a logarithmic scale between the values of 10^2 and 10^5. Based on negative controls, fluorescence levels around 10^2, 10^3, and 10^4-10^5 were considered negative, intermediate, and high, respectively.
For a detailed list of antibodies, please see supplementary table S1.

RNA expression analysis and qPCR

RNA was isolated with Arcturus® PicoPure™ RNA Isolation Kit (ThermoFisher Scientific) according to manufacturer's protocol including DNase digestion. Cells were directly sorted into 100 µl Lysis buffer, vortexed and stored at -80°C until RNA isolation. For reverse transcription, 9 µl purified RNA was incubated with 1 µl Oligo(dT)15 primers (Promega) at 80°C for 3 min. M-MLV buffer, M-MLV reverse transcriptase enzyme (200 U/ µl, Promega), dNTPs (10mM) and RNase-free water were added to RNA and Oligo(dT)15 mix to reach a final volume of 20 µl. cDNA synthesis was performed at 42°C for 60 min followed by 10 min at 80°C. cDNA was then preserved in -20°C until qPCR. mRNA levels for the genes of interest were measured using a StepOnePlus Real-time PCR system and TaqMan gene expression assays (Applied Biosystems): β-actin (ID: Mm01205647_g1), Tlx (ID: Mm00455855_m1), Hes1 (ID: Mm01342805_m), Hes5 (ID: Mm00439311_g1), Dll1 (ID: Mm01279269_m1), Jag1 (ID: Mm01270195_gh). Cycle threshold (Ct) values were each normalized to the respective β-actin value (= delta Ct (dCt)). Delta-delta Ct (ddCt) was calculated by subtracting dCt value of each population from the dCt of the $G^+P^+E^-$ population (normalizing population).

Intraventricular injections

WT mice were injected with 1 µL of adeno-associated virus (AAV) with a plasmid encoding short hairpin RNA targeting *Hes1* under the control of a U6 promoter, or a scramble sequence as control like previously described (Luque-Molina et al. 2019).

Immunofluorescence

Whole mount dissection and immunostaining was performed as previously described (Mirzadeh et al. 2008; Monaco et al. 2019).

For coronal sections, mice sedated with narcorene (400 mg/kg) were perfused with ice-cold phosphate-buffered saline (PBS) followed by 4% paraformaldehyde (PFA) in PBS, after which the brains were removed and postfixed in 3% PFA / 4% sucrose in PBS for 48h at 4°C. Brains were then cryoprotected by submersion in 30% sucrose in PBS at 4°C for 24h and sliced into 20-30 µm coronal sections using a Leica CM1950 cryostat (Leica Microsystems, Wetzlar, Germany). The sections were stored in PBS containing 0.01% sodium azide at 4°C until immunostaining.

Slices were permeabilized with 0.5% NP-40 in PBS for 5 min, then incubated in 10 mM glycine for 30 min for reduction of background fluorescence. Slices were blocked with 5% fetal calf serum (FCS) in PBS for 1h, and incubated with primary antibodies in PBS at 4°C overnight. After washing, secondary antibodies were applied in 5% FCS in PBS containing 4',6-diamidino-2-phenylindole (DAPI) for nuclear counterstain for 2h. Slices were then washed and mounted in mowiol. All steps were performed at room temperature if not otherwise indicated. Slices and whole mounts that were to be directly compared in regard to protein expression and fluorescence level were stained in parallel using the same antibodies and dilutions. Immunofluorescence on sorted cells was performed as previously described (Khatri et al. 2014). A detailed list of primary antibodies used is provided in supplementary table S2.

Imaging
Coronal sections and whole mounts were imaged using a Leica SP8 laser scanning confocal microscope. Images were acquired as z-stacks with 1 µm steps or 0.5-0.7 µm steps for cilia imaging. The imaging settings (laser intensity, gain, offset) were kept consistent for each experiment to assure comparability.

Statistical analysis
Immunopositive cells were counted and normalized to the total number of cells (identified by DAPI-stained nuclei) or as stated otherwise. For quantification of cells in the V-SVZ, we defined those cells as apical if their nuclei were located within the first two rows of nuclei bordering the lateral ventricle. Three regions of each slice were analysed, dorsal, lateral and ventral, in a 30,000 μm^2 -sized picture aligned with the longest axis of the apical side of the SVZ. Fiji/ImageJ software (Schindelin et al. 2012) was used for fluorescence intensity measurement and normalization to background levels. Ki67$^+$ cells were counted as bright if any point within the cell reached oversaturation.

During analysis, the pictures were labelled by treatment (i.e. doxycycline, DAPT, scramble/Hes1 shRNA, pregnancy) at all times and were not randomized or blinded.
Statistical significance was determined by two-tailed homoscedastic (or paired, when appropriate) Student's t-test for comparing two, and one-way or two-way ANOVA with Tukey's multiple comparisons test for comparing more than two datasets. The analyses were performed using Microsoft Excel or GraphPad Prism software. Significance was reached for * $p<0.05$, ** $p<0.01$, *** $p<0.001$. Graphs are represented as mean values ± SEM.

Results

The majority of G$^+$ cells display no apical membrane and Prominin-1-immunoreactivity

To label NSCs in the adult V-SVZ *in vivo*, we used 8-weeks-old (8W) hGFAP;H2B-GFP mice, in which the tetracycline-responsive transactivator (tTA) expressed from a human GFAP promoter controls in a Tet-off fashion the transcription of histone 2B fused to the green fluorescent protein (H2B-GFP), as described before (Luque-Molina et al. 2017). To further identify cells with an apical membrane, we labelled the apical side of the V-SVZ with DiI dye before tissue dissociation (Fig. 1A, B). Moreover, since Prominin-1 is prevalently expressed at the apical side of the niche in NSCs and ependymal cells (Khatri et al. 2014), cells were additionally immunostained with Prominin-1 antibodies before FACS analysis (Fig. 1D-F). As expected, H2B-GFP expressing (G$^+$) NSCs represented a small minority of total viable cells (Fig.1A). Nevertheless, compared to the remaining G$^-$ cells, they were significantly enriched in DiI$^+$ apical cells (Fig. 1B), which represented more than 23.54% ± 2.62 of the total DiI$^+$ cells (Fig. 1C). Similarly, the incidence of Prominin-1-immunopositive (P$^+$) cells was higher in the G$^+$ population than in the remaining G$^-$ cells (Fig. 1E), and G$^+$P$^+$ cells were composed mostly of DiI$^+$ cells (Fig. 1F), which is consistent with Prominin-1 being

prominently expressed in apical V-SVZ cells. However, the majority of H2B-GFP tagged cells did not express Prominin-1 (G^+P^-) or DiI labelling (Fig. 1F), indicating that they are basal progenitors lacking an apical attachment. To further characterize the two populations of apical and basal progenitors, we next investigated the colocalization of the H2B-GFP signal and immunoreactivity to Nestin (Fig. 2A, B), whose expression is particularly high in actively cycling NSCs (Codega et al. 2014), and GFAP (supplementary Fig. S1). For this analysis, we performed double immunostaining on coronal sections of brains obtained from 8W hGFAP;H2B-GFP mice. Moreover, in order to increase the percentage label-retaining cells within the reporter expressing population, mice were either administered doxycycline in the drinking water for 30 days or left untreated for the same period before being sacrificed for analysis (Fig. 2A, B). Consistent with our FACS data, we found that in the absence of doxycycline, most G^+ cells localize at the basal side of the niche and do not display Nestin or GFAP immunoreactivity. In contrast, $Nestin^+$ and $GFAP^+$ cells were mostly observed at the apical side of the niche (Fig. 2B, and supplementary Fig. S1A, B), where double immunopositive $G^+Nestin^+$ cells represented 45% of the total apical G^+ cells. The same analysis in mice treated with doxycycline revealed a significant decrease only in the number of apical $G^+Nestin^+$ and G^+GFAP^+ cells. Notably, Nestin and GFAP expression decreased only within the subset of G^+ apical cells (Fig. 2B), indicating that either filament protein immunoreactivity is detectable in only apical G^+ cells undergoing proliferation.

Primary cilia are closely linked to cell cycle progression and signal transduction (Goto, Inoko, and Inagaki 2013). However, not all adult NSCs in the V-SVZ display primary cilia (Khatri et al. 2014). We therefore used adenylate cyclase 3 (AC3) as a primary cilia marker (Monaco et al. 2019; Bishop et al. 2007) in combination with Nestin and H2B-GFP to assess which marker protein is expressed in ciliated cells (Fig. 2C, E). In this analysis, only reporter- and/or Nestin-expressing cells were counted to restrict the analysis to neural precursors. Most ciliated precursors were located at the apical side of the V-SVZ, where an average of 4.78±1.79% of apical cells display a primary cilium vs only 0.7±0.31% of the basal cells (Fig. 2C, D). Furthermore, around 50% of the ciliated cells were G^+ apical precursors of which most (33.21±18.8% of total ciliated cells) co-expressed Nestin (Fig. 2E). In contrast, only few basal cells extended a primary cilium and the majority (66.75±28%) consisted of $G^+Nestin^-$ cells (Fig. 2E). A similar association between apical NSCs and primary cilia was observed in WT mice by analysis of primary cilia on FACS sorted V-SVZ cells (supplementary Fig. S2), as reported before (Khatri et al. 2014). We found that, independent of Prominin-1 expression, most ciliated cells are apical (DiI^+) cells and that the majority of basal G^+ cells are non-ciliated. Taken together, these data show that apical and basal G^+ cells display different intermediate filament expression and cilia extension, suggesting that the two pools of NSCs differentially sense and respond to environmental signals.

Both apical and basal G^+ cells display hallmarks of stem cells

We next investigated whether basal progenitors undergo quiescence. For this analysis, we measured the number of label-retaining cells in each population by quantifying the number of total G^+ cells in the V-SVZ of hGFAP;H2B-GFP control mice, and animals

which had been given doxycycline in the drinking water for a month, which leads to the disappearance of the fluorescent nuclear signal after five cell divisions (Waghmare et al. 2008; Luque-Molina et al. 2017). After quantification we observed a small effect of the treatment, which causes a significant reduction only in G^+ cells located at the basal side of the niche (Fig. 3A, B). This indicates that both basal and especially apical progenitors consist of quiescent or slow cycling label-retaining cells. Supporting this conclusion, the majority of apical and basal G^+ cells did not display Ki67 immunoreactivity (Fig. 3C). However, the proportion of $Ki67^+$ cycling cells was similar, i.e. around 45%, within apical and basal G^+ cells. This shows that the difference in the number of label-retaining cells between apical and basal G^+ cells reflects faster cell divisions in the latter compared to the first, rather than a difference in the content of quiescent cells between the two populations. Consistent with this hypothesis, Ki67 expression was significantly reduced in basal but not apical G^+ cells upon doxycycline administration, as expected if basal $Ki67^+$ cycling cells were to undergo more cell divisions than their apical counterpart during the chasing period.

Self-renewal is a defining property of stem cells and we next investigated self-renewal of apical and basal G^+ cells *in vivo* using hGFAP;H2B-GFP mice. We reasoned that in the absence of doxycycline, the expression of the H2B-GFP reporter would be downregulated only in cells undergoing non-renewing cell divisions. Thus, in control untreated mice, self-renewal would maintain high levels of fluorescence expression in the pool of G^+ cells, whereas non-renewing cell division, comparable to doxycycline administration, would cause a dilution in fluorescence levels at each cell division. Therefore, instead of quantifying total G^+ cells as above, to measure self-renewal rate, we compared the percentage of G^+ cells expressing high (G^h) or intermediate (G^i) fluorescence levels, as described before (Luque-Molina et al. 2017, see also “Methods” section), in apical P^+G^+ and basal P^-G^+ progenitors isolated from the control and doxycycline treated hGFAP;H2B-GFP mice (Fig. 3D). This analysis revealed that doxycycline administration led to a consistent decrease in the percentage of G^h cells within apical and especially basal precursors, paralleled in both populations by a correspondent increase in the proportion of G^i cells. Thus, both apical and basal precursors undergo *in vivo* self-renewing divisions.

Neurosphere formation is a hallmark of actively proliferating adult NSCs (Khatri et al. 2014; Codega et al. 2014). Therefore, we next used clonal assays to test the ability of apical and basal neural G^+ precursors to form neurospheres (supplementary Fig. S3C). For this analysis, cells were additionally sorted between those expressing high (E^h) and low (E^l) EGFR levels, as the first are enriched in clone forming cells compared to the latter (Ciccolini et al. 2005). In the absence of doxycycline, clones were generated by both basal $G^+P^-E^h$ and $G^+P^-E^l$ progenitors, albeit at a lower rate. In contrast, at the apical side, only $G^+P^+E^h$ progenitors underwent clone formation, consistent with the fact that $G^+P^+E^l$ cells consist largely of label-retaining cells (Khatri et al. 2014). Moreover, when isolating G^+ cells from mice treated with doxycycline, clone formation was mainly observed in $G^+P^-E^+$ cells, supporting the notion that long-term quiescent NSCs do not form clones. These data indicate that, although basal NSCs undergo faster cell cycle kinetics than apical NSCs, they are not rapidly proliferating intermediate precursors. Taken together, we found that basal G^+ precursors display

characteristics of adult NSCs, including the ability to undergo quiescence, self-renewal, and clone formation when they are in an active state. Therefore, they will be hereafter referred to as basal NSCs.

Basal NSCs represent the predominant NSC population throughout postnatal life

It has been recently shown that with age apical NSCs lose their apical attachment, giving rise to more differentiated basal progenitors (Obernier et al. 2018). Therefore, we next investigated if basal progenitors are generated during adulthood or already present in the neonatal brain. We first analysed the presence of apical and basal NSCs in slices of the SVZ of 1W-old hGFAP;H2B-GFP mice (supplementary Fig. S4). Quantitative analysis showed not only the presence of both apical and basal G^+ NSCs already at this early age, but also similar differences between the two groups with respect to Nestin expression (supplementary Fig. S4A, B) and primary cilia extension (supplementary Fig. S4A, C) which were already observed in adult mice. Moreover, in the neonatal V-SVZ, G^+ cells also represented almost half of the total ciliated cells (supplementary Fig. S4D). However, apical neonatal cells displayed a greater proportion of G^+ cells co-expressing Nestin and extending a primary cilium than the 8W-old counterpart. Taken together, these data show that cells with defining characteristics of basal and apical NSCs are present at early postnatal ages. To obtain a more dynamic overview of these changes, we then quantified the number of apical G^+P^+ and basal G^+P^- at various postnatal ages (Fig. 4A left panel). In addition, we investigated both apical and basal NSC activation at each age, by measuring the percentage of cells expressing high EGFR at the cell surface (E^h) in each NSC group (Fig. 4A right panel). Consistent with previous reports (Carrillo-Garcia et al. 2010), we observed a decrease in the number of basal and especially apical NSCs with age. However, the sharpest and only significant drop in NSC numbers occurred between 1 and 2 weeks of postnatal age. In contrast, the proportion of activated NSCs underwent a first significant decrease in young adult mice and it concerned uniquely basal NSCs. However, activation was significantly reduced in both apical and basal NSCs (Fig. 4A) in old (25 weeks) animals. To further investigate age-related changes in stemness, we next determined the effect of age on proliferation and self-renewal potential of apical and basal NSCs by means of clonal assays (Fig. 4B-D). For this analysis, apical and basal NSCs were isolated from the V-SVZ of 8W and 25-30W old animals by flow cytometry, based on DiI labelling and both EGFR and Prominin-1 immunoreactivity. Consistent with our observations above, age led to a decrease in the number of activated NSCs $G^+P^-E^h$ within the basal (D^-) but not apical (D^+) pool of NSCs (Fig. 4B). At both ages, all types of NSCs generated clones and in line with our findings *in vivo*, they were also able to undergo self-renewal *in vitro*, measured by the number of green cells per clone (Fig. 4C and D). However, unlike the remaining populations, apical $G^+P^+E^h$ NSCs isolated from older mice generated only small clones (Fig. 4D) and underwent very limited self-renewal. In addition, in both apical and basal NSCs, age led to a loss of clonal activity within Prominin-1 immunopositive NSCs paralleled by an increase in the number of Prominin-1 immunonegative cells giving rise to small clones (Fig. 4D). Thus, throughout adulthood, basal NSCs represent the major NSC population in the postnatal V-SVZ although the number of basal and especially apical

NSCs undergoes a strong reduction during the second postnatal week. Hence, NSC activation and self-renewal are differentially affected by age in apical and basal NSCs.

Basal NSCs derive from apical NSCs and are the main contributors to neurogenesis

Having shown that apical and basal NSCs are present throughout adulthood in the V-SVZ, we next investigated their lineage relationship and their respective contribution to adult neurogenesis. For example, although we have previously shown that most OB adult born interneurons are derived from NSCs in the V-SVZ tagged with a minimal GFAP promoter (Weber et al. 2011), the promoter is active in both apical and basal cells (data not shown). Therefore, it is not clear whether both pools of NSCs contribute to neurogenesis. To address these points, we selectively tagged apical V-SVZ cells by intraventricular injection of recombinant adenovirus associated viral (AAV) particles expressing GFP in adult WT mice, as reported before (Luque-Molina et al. 2019). We first used this approach to investigate the lineage relationship between apical and basal NSCs. Analysis of coronal brain slices 14 days after injection showed that the overwhelming majority of GFP^+ cells were represented by apical cells (supplementary Fig. S5A, B). Moreover, the rare basal GFP^+ cells were virtually all non-cycling as no Ki67-expressing cells were detected (supplementary Fig. S5C). Analysis of brain slices 6 weeks post viral injection showed no significant change in the number of apical and basal GFP^+ cells between the two time points (supplementary Fig. S5B). To further investigate the nature of the labelled cells, we next quantified the expression of the Sex-determining region Y (SRY)-box transcription factor 9 (Sox9), which is expressed in multipotent NSCs (Scott et al. 2010), and GFAP in apical and basal cells (Fig. 5A, B) in the V-SVZ 6 weeks after virus injection. At the apical side of the niche, most GFP^+ cells also expressed Sox9, consistent with previous observations showing the expression of the transcription factor in most ependymal cells (Scott et al. 2010; Sun et al. 2017). However, after 6 weeks, a consistent portion of apical GFP^+ cells displayed an antigenic profile of NSCs, i.e. expressing both GFAP and or Sox9, confirming that our approach targets apical NSCs (Fig. 5B). In contrast, on the basal side of the niche, very few cells expressed either marker, showing that the contribution of apical cells to the pool of basal NSCs is very limited. To investigate neurogenesis, we next quantified the change in expression of doublecortin (DCX) in the OB of injected mice (Fig. 5C, D). At both ages, we could find three types of labelled cells in the OB: cells with neuronal morphology expressing GFP only or both DCX and GFP, and the vast majority of immature neurons labelled with only DCX. Independent of age, both types of GFP^+ cells represented a very small percentage of total cells especially in the core of the OB where newly generated neurons switch migration mode (supplementary Fig. S5D). Consistent with previous observations (Nkomozepi, Mazengenya, and Ihunwo 2019), the number of DCX^+ cells significantly decreased with age, whereas the number of either GFP^+ cells did not significantly change. Taken together, our data show that, within a six-week period, apical NSCs generate few basal cells in the SVZ with antigenic characteristics of NSCs and rare OB interneurons. However, in normal conditions, the contribution of apical NSCs to the generation of basal NSCs may be difficult to detect due to apical NSCs undergoing very rare cell divisions in the adult

stage. Therefore, we next investigated whether apical and/or basal NSCs contribute to the physiological increase in the number of NSCs, which is elicited in female mice by giving birth and lactation (Shingo et al. 2003). For this, we quantified apical and basal NSCs by flow cytometry, in the V-SVZ of female hGFAP;H2B-GFP virgin mice and littermate animals which had just given birth (Fig. 5E-G). This analysis revealed that the number of G^+ NSCs was significantly increased in mice which had been recently pregnant (preg) compared to the control (virgin, virg; Fig. 5E). Moreover, this was due to a significant increase in the number of total basal $G^+P^-D^-$ cells (Fig. 5F), whereas the number of apical NSCs was not significantly altered (Fig. 5G), showing that pregnancy affects only the number of basal but not apical NSCs. Thus, apical NSCs do not seem to respond to physiological stimuli which promote NSC activity, and generation of extra OB interneurons which reveals their highly quiescent nature.

Regulators of NSC activation are differentially expressed in apical and basal NSCs

We have recently found that the TLX/NR2E1-Notch axis coordinates activation and proliferation between apical and basal progenitors in the V-SVZ regulating Notch signaling activation across the V-SVZ (Luque-Molina et al. 2019). However, the molecular basis underlying this regulation is still poorly understood. To investigate this issue, we used quantitative RT-PCR to compare the expression of *Tlx* and various Notch signaling-related gene transcripts in apical $G^+P^+E^l$ and basal $G^+P^-E^l$ quiescent NSCs, in both $G^+P^+E^h$ and $G^+P^-E^h$ activated NSCs and in $G^-P^-E^h$ transit-amplifying progenitors (TAPs; Fig. 6). Consistent with previous analyses (Obernier et al. 2011; Li et al. 2012), we found that the expression of *Tlx* was greatly increased in apical activated $G^+P^+E^h$ NSCs as well as in $G^-P^-E^h$ TAPs. In contrast, a significant change in *Tlx* expression was not detected in either quiescent $G^+P^-E^l$ or activated $G^+P^-E^h$ basal NSCs (Fig. 6B), indicating that the increase in the expression of the orphan receptor is associated prominently with activation of apical but not basal NSC activation. Analysis of the trannscript levels of the main Notch ligands, i.e. *Delta1* (*Dll1*; Fig. 6C) and *Jagged 1* (*Jag1*; Fig. 6D), and of the most prominent Notch effector genes in the V-SVZ, i.e. *Hes1* (Fig. 6E) and *Hes5* (Fig. 6F), also revealed different expression profiles between activated and quiescent apical and basal NSCs. The lowest levels of gene expression, including both Notch ligands analysed, were observed in apical quiescent $G^+P^+E^l$ NSCs. Basal quiescent $G^+P^-E^l$ cells also displayed low levels of *Dll1* expression, but significantly higher expression of *Jag1* than the apical group, although significance was only observed upon direct comparison between the two populations. Consistent with previous findings (Kawaguchi et al. 2013), in both apical and basal NSCs, the expression levels of Notch ligands were positively correlated with NSC activation (Fig. 6C, D). Additional differences between apical and basal progenitors were observed with respect to the expression of effector genes. The levels of *Hes1* transcripts were upregulated in a comparable manner across the four remaining cell populations, whereas *Hes5* expression was increased only in basal cells, including TAPs (Fig. 6E, F). Taken together, these data show a distinct distribution of genes associated with Notch signaling along the apical/basal axis of the V-SVZ. They also show that at both sides of the niche NSC activation leads to the acquisition of a

transcriptional profile which is a characteristic of Notch signal sending NSCs, whereas quiescent NSCs, especially at the apical side, essentially display a signature of Notch signal receiving NSCs. Supporting this last conclusion, we also found that Notch signaling activation was stronger in ciliated apical cells including ependymal as well as NSCs (supplementary Fig. S6). Since the Tlx-Hes1 axis plays a role in the activation of apical NSCs, we next downregulated Hes1 expression specifically in apical NSCs to determine the effect on Notch activation and proliferation dynamics in apical and basal NSCs. Therefore, we intraventricularly injected an AAV constitutively expressing GFP and either a Hes1-specific short hairpin (AAV-Hes1-sh) or a scramble control (AAV-sc-sh), as described before (Luque-Molina et al. 2019). Using this approach, beside apical NSCs, we also target ependymal cells, which also express Hes-1(Stratton et al. 2019). Thus, we used meta-analysis of the RNA-sequencing data collected and made available by the lab of Sten Linnarsson at Karolinska Institute, Sweden (Zeisel et al. 2018), on mousebrain.org to investigate Hes-1 expression in ependymal cells (Supplementary Fig. S7). We found that within the ependymal population the expression of Hes1 was limited to a group of progenitor-like cells characterized by the expression of NSC marker Nestin, with or without GFAP, (Supplementary Fig. S7A, B) and that this population expressed highest levels of radial glia markers within the ependymal population (Supplementary Fig. S7C). Taken together, these data indicate that at the apical side of the niche, Hes1 is expressed essentially in NSCs and not in mature ependymal cells. We therefore next investigated the effect of apical loss of Hes1 function via the AAV-GFP tagged intraventricular injection (Fig. 7). Independent of the injected constructs, 14 days after intraventricular injection, GFP was expressed mainly by cells lining the lateral ventricle, most of which represented ependymal cells (Fig. 7A, B). We next measured fluorescence levels of the Notch intracellular domain (NICD; Fig. 7A, C), to quantify activation of Notch signaling, and Ki67 expression (Fig. 7B- D), to measure the number of cycling cells in infected (GFP^+) and non-infected (GFP^-) apical and basal SVZ cells. This analysis showed that, compared to the scramble control, injection of AAV-Hes1-sh affected NICD immunoreactivity across all groups examined including basal cells, showing that Notch signaling connects progenitor cells between the apical and basal sides of the niche. Downregulation of Notch signaling was accompanied by an increase in the number of cycling cells ($Ki67^+$) across all the populations examined, albeit this effect was stronger in apical than in basal cells (Fig. 7D). Moreover, the increase of proliferation, even at the apical side, was essentially observed in GFP^- but not GFP^+ infected cells, further underscoring the importance of cell-cell interactions. Taken together, these data show that in the V-SVZ, Notch signaling connects apical and basal progenitors, thereby repressing their proliferation. However, this type of manipulation did not allow us to observe the immediate consequences of downregulation of Notch signaling in apical and basal NSCs. Therefore, we next exposed the whole V-SVZ dissected from 8W-old hGFAP;H2B-GFP to the γ-secretase inhibitor DAPT (N-[N-(3,5-difluorophenacetyl)-L-alanyl]-S-phenylglycine t-butyl ester) or the solvent dimethyl sulfoxide (DMSO) as a control, for 24 hours before fixation and immunostaining with antibodies against Nestin and Ki67 (Fig. 7E, H). The treatment with DAPT resulted in an overall increase of bright $Ki67^+$ (Fig. 7F) and mitotic cells, i.e. cells in meta- or

anaphase (Fig. 7G). Blockade of Notch signaling also led to a significant increase in the percentage of $G^+Nestin^+$ and $G^+Ki67^+Nestin^+$ triple positive cells in the G^+ population (Fig. 7H-J). Notably, these effects were only significant at the apical and not at the basal side of the niche, supporting the view that inhibition of Notch signaling primarily affects apical NSCs. Taken together, these data show that Notch signaling counteracts cell cycle progression of apical progenitors and that this regulation is transmitted from the apical to the basal side of the niche through Notch-mediated lateral inhibition.

Discussion

In this study we show the presence of basal NSCs in the adult V-SVZ of the mouse brain for the first time. Notably, our data show that whereas basal NSCs are responsible for the generation of most adult-born interneurons in the OB, apical NSCs contribute essentially as gate-keepers to neurogenesis by receiving Notch-mediated lateral inhibition of proliferation from surrounding activated progenitors which express Notch ligands, Dll1 and Jag1. It is established that Notch signaling is essential to maintain stemness during quiescence (Imayoshi et al. 2010; Kawaguchi et al. 2013; Kawai et al. 2017; Than-Trong et al. 2018) and to control niche homeostasis by coordinating proliferation of adult NSCs and more differentiated progenitors (Wang et al. 2009; Aguirre, Rubio, and Gallo 2010). However, the mechanisms underlying this regulation are still not clear. We here show that underlying this function of Notch signaling is a distinctive distribution of Notch ligands, thereby their lowest levels of expression are observed in apical quiescent NSCs, and the highest in activated NSCs and TAPs. We propose that this interaction between Notch-sending and receiving cells is a key mechanism regulating the overall behaviour of adult NSCs and niche homeostasis. An increase in the expression of Notch ligands accompanying the progression of progenitors along the neural lineage was already reported (Kawaguchi et al. 2013). Our data complement these observations by showing that apical quiescent NSCs, unlike their basal counterpart, display a signature of Notch receiving cells. This difference results in a gradient of Notch activation along the apical/basal axis which regulate proliferation across the V-SVZ. Using specific interference in apical NSCs with the knock-down of Hes1, we were able not only to lower Notch activation across the whole niche, but also to promote proliferation and NSCs activation at both apical and basal sides of the niche. We have previously shown that downregulation of Hes1 also led to diminished Notch activation and increased proliferation in the V-SVZ of $Tlx^{-/-}$ mice (Luque-Molina et al. 2019). However, unlike in WT mice studied here, in mutant mice it was found that downregulation of Notch signaling concerned only cells at the apical side of the niche, whereas increase in proliferation was prevalently associated with basal progenitors. The difference in the pattern of proliferation between the two genotypes may reflect the greater role that Tlx plays in activated apical NSCs and TAPs, where the orphan nuclear receptor is prevalently expressed. Since they are absent in $Tlx^{-/-}$ mice, the fact that we did not observe downregulation of Notch activation in mutant mice upon Hes1 loss of function may reflect the fact that activated apical NSCs and TAPs are necessary to transmit Notch signaling across the apical/basal axis

of the niche. However, we cannot exclude the possibility that Hes1 expression, which in the absence of Tlx is also increased in basal progenitors, prevents the downregulation of Notch activation in this population.

The identity of NSCs in the V-SVZ has been object of numerous studies. Although the first attempts at NSC identification disagreed on the nature of NSCs, they both proposed apical cells as the main source of neurogenesis in the adult brain (Doetsch et al. 1999; Johansson et al. 1999). Despite the increasing range of approaches and markers used in earlier studies, the view that adult NSCs represent radial glia-like cells, has been maintained (Beckervordersandforth et al. 2010; Codega et al. 2014; Nam and Capecchi 2020). In contrast with this view, we here provide several lines of evidence of the additional existence of basal NSCs in the adult V-SVZ. Firstly, apical and basal NSCs can be both tagged using a human GFAP promoter, which unlike the murine counterpart (Weber et al. 2011) is active in embryonic radial glia as well as adult NSCs in mice (Zhuo et al. 2001; Malatesta et al. 2003; Anthony et al. 2004; Anthony and Heintz 2008). Secondly, basal NSCs, like their apical counterpart, undergo prolonged quiescence and are capable of extensive self-renewal *in vivo* and *in vitro*. Thirdly, we found that basal NSCs are the most abundant NSC population throughout postnatal development as they constituted the majority of reporter expressing cells. Previous work of transcriptional characterization of cells in the adult V-SVZ has also provided evidence of the presence of different pools of NSCs (Mich et al. 2014; Dulken et al. 2017; Luo et al. 2015). However, this work did not investigate the localization of the various NSC pools in the niche, associating the existence of the various NSC pools essentially with different degrees of quiescence and activation. Our observation that basal and apical NSCs also display differences in rate of cell cycle progression provides additional insight for the interpretation of these previously reported data. Moreover, it also provides a more unified view of the spatial organization of different pools of adult NSCs in the two main neurogenic niches. The presence of morphologically distinct types of NSCs, i.e. type 1 and type 2 (Steiner et al. 2006), has been long studied in the in the SGZ. Although both pools of hippocampal NSCs express radial glial markers in addition to Sox2 and Sox9 transcription factors (Suh et al. 2007; Sun et al. 2017), they are morphologically distinct, as only type 1 cells display a typical radial glia morphology with apical-basal polarity (Seri et al. 2001). In striking similarity with the differences between apical and basal NSCs in the V-SVZ reported here, it was observed that in the SGZ, type 1 radial NSCs consistently display Nestin and GFAP immunoreactivity although they are largely quiescent (Sun et al. 2017). In fact, in the adult SGZ, the expression of proliferation markers was mainly observed in non-radial NSCs, which like basal NSCs in the V-SVZ are the main contributors to steady-state neurogenesis and can actively proliferate in response to physiological stimuli (Lugert et al. 2010).

Although being widely considered as a NSC marker, Nestin expression is not always observed in NSCs, and it has been previously suggested that quiescence is associated with a loss of Nestin expression in adult NSCs in the V-SVZ (Codega et al. 2014). Indeed, we here found that Nestin expression is significantly downregulated in quiescent apical NSCs and with increasing age. However, in adult basal NSCs, Nestin

expression is virtually absent, independent of the state of activation. Moreover, in the SGZ, Nestin is also expressed in radial NSCs, which are largely quiescent (Kempermann et al. 2004; Encinas, Vaahtokari, and Enikolopov 2006), suggesting additional mechanisms of regulation of Nestin expression in NSCs. Notably, unlike in the V-SVZ, NSCs and progenitors in the SGZ all display primary cilia (Breunig et al. 2008; Amador-Arjona et al. 2011). Since we here found that very few basal NSCs extend primary cilia and express Nestin, it is possible that the expression of Nestin is mediated by cilia-dependent signals. In the V-SVZ, primary cilia do not only regulate quiescence in radial glia and adult NSCs (Beckervordersandforth et al. 2010; Khatri et al. 2014), but they are also key to sensing signals present in the cerebrospinal fluid filling the ventricular cavity (Silva-Vargas et al. 2016; Monaco et al. 2019). Consistent with this view, recent observations have highlighted that in the V-SVZ, acquisition of quiescence concerns a prolonged time period (Borrett et al. 2020) and involves different stages and integration of multiple regulatory signals.
Our data contribute to understanding the complexity of the adult NSC niche by showing that the V-SVZ contains two pools of NSCs which are exposed to different microenvironments and are differentially prepared to sense it.

Acknowledgements

K.B. was supported by the Interdisciplinary Center for Neuroscience (IZN) and the Landesgraduiertenförderung (LGF) of the Heidelberg University Graduate Academy. The authors would like to thank Inma Luque-Molina for her help with clonal analysis. We would also like to thank the Department of Neurobiology for its continued support.

Author contributions

Conceptualization, Methodology, Funding Acquisition: F.C.; Formal analysis: K.B., Y.A. and F.C.; Investigation: K.B., Y.A., C.M., G.H.-W., Y.S., U.E., P.K. and F.C.; Writing – original draft: F.C., K.B. and Y.A.; Writing – review and editing: F.C., K.B., Y.A., Y.S., U.E. and P.K.; Visualization: K.B. and Y.A.

References

Aguirre, A., M. E. Rubio, and V. Gallo. 2010. 'Notch and EGFR pathway interaction regulates neural stem cell number and self-renewal', *Nature*, 467: 323-7.

Altman, J. 1962. 'Are new neurons formed in the brains of adult mammals?', *Science*, 135: 1127-8.

Altman, J., and G. D. Das. 1965. 'Post-natal origin of microneurones in the rat brain', *Nature*, 207: 953-6.

Alves, J. A., P. Barone, S. Engelender, M. M. Froes, and J. R. Menezes. 2002. 'Initial stages of radial glia astrocytic transformation in the early postnatal anterior subventricular zone', *J Neurobiol*, 52: 251-65.

Amador-Arjona, A., J. Elliott, A. Miller, A. Ginbey, G. J. Pazour, G. Enikolopov, A. J. Roberts, and A. V. Terskikh. 2011. 'Primary cilia regulate proliferation of amplifying progenitors in adult hippocampus: implications for learning and memory', *J Neurosci*, 31: 9933-44.

Anthony, T. E., and N. Heintz. 2008. 'Genetic lineage tracing defines distinct neurogenic and gliogenic stages of ventral telencephalic radial glial development', *Neural Dev*, 3: 30.

Anthony, T. E., C. Klein, G. Fishell, and N. Heintz. 2004. 'Radial glia serve as neuronal progenitors in all regions of the central nervous system', *Neuron*, 41: 881-90.

Beckervordersandforth, R., P. Tripathi, J. Ninkovic, E. Bayam, A. Lepier, B. Stempfhuber, F. Kirchhoff, J. Hirrlinger, A. Haslinger, D. C. Lie, J. Beckers, B. Yoder, M. Irmler, and M. Gotz. 2010. 'In vivo fate mapping and expression analysis reveals molecular hallmarks of prospectively isolated adult neural stem cells', *Cell Stem Cell*, 7: 744-58.

Bishop, G. A., N. F. Berbari, J. Lewis, and K. Mykytyn. 2007. 'Type III adenylyl cyclase localizes to primary cilia throughout the adult mouse brain', *J Comp Neurol*, 505: 562-71.

Borrett, M. J., B. T. Innes, D. Jeong, N. Tahmasian, M. A. Storer, G. D. Bader, D. R. Kaplan, and F. D. Miller. 2020. 'Single-Cell Profiling Shows Murine Forebrain Neural Stem Cells Reacquire a Developmental State when Activated for Adult Neurogenesis', *Cell Rep*, 32: 108022.

Breunig, J. J., M. R. Sarkisian, J. I. Arellano, Y. M. Morozov, A. E. Ayoub, S. Sojitra, B. Wang, R. A. Flavell, P. Rakic, and T. Town. 2008. 'Primary cilia regulate hippocampal neurogenesis by mediating sonic hedgehog signaling', *Proc Natl Acad Sci U S A*, 105: 13127-32.

Brill, M. S., J. Ninkovic, E. Winpenny, R. D. Hodge, I. Ozen, R. Yang, A. Lepier, S. Gascon, F. Erdelyi, G. Szabo, C. Parras, F. Guillemot, M. Frotscher, B. Berninger, R. F. Hevner, O. Raineteau, and M. Gotz. 2009. 'Adult generation of glutamatergic olfactory bulb interneurons', *Nat Neurosci*, 12: 1524-33.

Carrillo-Garcia, C., Y. Suh, K. Obernier, G. Holzl-Wenig, C. Mandl, and F. Ciccolini. 2010. 'Multipotent precursors in the anterior and hippocampal subventricular zone display similar transcription factor signatures but their proliferation and maintenance are differentially regulated', *Mol Cell Neurosci*, 44: 318-29.

Cesetti, T., K. Obernier, C. P. Bengtson, T. Fila, C. Mandl, G. Holzl-Wenig, K. Worner, V. Eckstein, and F. Ciccolini. 2009. 'Analysis of stem cell lineage progression in the neonatal subventricular zone identifies EGFR+/NG2- cells as transit-amplifying precursors', *Stem Cells*, 27: 1443-54.

Ciccolini, F., C. Mandl, G. Holzl-Wenig, A. Kehlenbach, and A. Hellwig. 2005. 'Prospective isolation of late development multipotent precursors whose migration is promoted by EGFR', *Dev Biol*, 284: 112-25.

Codega, P., V. Silva-Vargas, A. Paul, A. R. Maldonado-Soto, A. M. Deleo, E. Pastrana, and F. Doetsch. 2014. 'Prospective identification and purification of quiescent adult neural stem cells from their in vivo niche', *Neuron*, 82: 545-59.

Doetsch, F., I. Caille, D. A. Lim, J. M. Garcia-Verdugo, and A. Alvarez-Buylla. 1999. 'Subventricular zone astrocytes are neural stem cells in the adult mammalian brain', *Cell*, 97: 703-16.

Doetsch, F., J. M. Garcia-Verdugo, and A. Alvarez-Buylla. 1997. 'Cellular composition and three-dimensional organization of the subventricular germinal zone in the adult mammalian brain', *J Neurosci*, 17: 5046-61.

———. 1999. 'Regeneration of a germinal layer in the adult mammalian brain', *Proc Natl Acad Sci U S A*, 96: 11619-24.

Dulken, B. W., D. S. Leeman, S. C. Boutet, K. Hebestreit, and A. Brunet. 2017. 'Single-Cell Transcriptomic Analysis Defines Heterogeneity and Transcriptional Dynamics in the Adult Neural Stem Cell Lineage', *Cell Rep*, 18: 777-90.

Encinas, J. M., A. Vaahtokari, and G. Enikolopov. 2006. 'Fluoxetine targets early progenitor cells in the adult brain', *Proc Natl Acad Sci U S A*, 103: 8233-8.

Feierstein, C. E. 2012. 'Linking adult olfactory neurogenesis to social behavior', *Front Neurosci*, 6: 173.

Florio, M., and W. B. Huttner. 2014. 'Neural progenitors, neurogenesis and the evolution of the neocortex', *Development*, 141: 2182-94.

Fuentealba, L. C., S. B. Rompani, J. I. Parraguez, K. Obernier, R. Romero, C. L. Cepko, and A. Alvarez-Buylla. 2015. 'Embryonic Origin of Postnatal Neural Stem Cells', *Cell*, 161: 1644-55.

Furuta, M., and R. S. Bridges. 2005. 'Gestation-induced cell proliferation in the rat brain', *Brain Res Dev Brain Res*, 156: 61-6.

Furutachi, S., H. Miya, T. Watanabe, H. Kawai, N. Yamasaki, Y. Harada, I. Imayoshi, M. Nelson, K. I. Nakayama, Y. Hirabayashi, and Y. Gotoh. 2015. 'Slowly dividing neural progenitors are an embryonic origin of adult neural stem cells', *Nat Neurosci*, 18: 657-65.

Gage, F. H. 2002. 'Neurogenesis in the adult brain', *J Neurosci*, 22: 612-3.

Garcia, A. D., N. B. Doan, T. Imura, T. G. Bush, and M. V. Sofroniew. 2004. 'GFAP-expressing progenitors are the principal source of constitutive neurogenesis in adult mouse forebrain', *Nat Neurosci*, 7: 1233-41.

Goto, H., A. Inoko, and M. Inagaki. 2013. 'Cell cycle progression by the repression of primary cilia formation in proliferating cells', *Cell Mol Life Sci*, 70: 3893-905.

Hockfield, S., and R. D. McKay. 1985. 'Identification of major cell classes in the developing mammalian nervous system', *J Neurosci*, 5: 3310-28.

Hu, X. L., G. Chen, S. Zhang, J. Zheng, J. Wu, Q. R. Bai, Y. Wang, J. Li, H. Wang, H. Feng, J. Li, X. Sun, Q. Xia, F. Yang, J. Hang, C. Qi, T. N. Phoenix, S. Temple, and Q. Shen. 2017. 'Persistent Expression of VCAM1 in Radial Glial Cells Is Required for the Embryonic Origin of Postnatal Neural Stem Cells', *Neuron*, 95: 309-25 e6.

Imayoshi, I., M. Sakamoto, M. Yamaguchi, K. Mori, and R. Kageyama. 2010. 'Essential roles of Notch signaling in maintenance of neural stem cells in developing and adult brains', *J Neurosci*, 30: 3489-98.

Johansson, C. B., S. Momma, D. L. Clarke, M. Risling, U. Lendahl, and J. Frisen. 1999. 'Identification of a neural stem cell in the adult mammalian central nervous system', *Cell*, 96: 25-34.

Kalman, M., and M. B. Pritz. 2001. 'Glial fibrillary acidic protein-immunopositive structures in the brain of a Crocodilian, Caiman crocodilus, and its bearing on the evolution of astroglia', *J Comp Neurol*, 431: 460-80.

Kawaguchi, D., S. Furutachi, H. Kawai, K. Hozumi, and Y. Gotoh. 2013. 'Dll1 maintains quiescence of adult neural stem cells and segregates asymmetrically during mitosis', *Nat Commun*, 4: 1880.

Kawai, H., D. Kawaguchi, B. D. Kuebrich, T. Kitamoto, M. Yamaguchi, Y. Gotoh, and S. Furutachi. 2017. 'Area-Specific Regulation of Quiescent Neural Stem Cells by Notch3 in the Adult Mouse Subependymal Zone', *J Neurosci*, 37: 11867-80.

Kempermann, G., S. Jessberger, B. Steiner, and G. Kronenberg. 2004. 'Milestones of neuronal development in the adult hippocampus', *Trends Neurosci*, 27: 447-52.

Khatri, P., K. Obernier, I. K. Simeonova, A. Hellwig, G. Hölzl-Wenig, C. Mandl, C. Scholl, S. Wolfl, J. Winkler, J. A. Gaspar, A. Sachinidis, and F. Ciccolini. 2014. 'Proliferation and cilia dynamics in neural stem cells prospectively isolated from the SEZ', *Sci Rep*, 4: 3803.

Kriegstein, A. R., and M. Gotz. 2003. 'Radial glia diversity: a matter of cell fate', *Glia*, 43: 37-43.

Li, S., G. Sun, K. Murai, P. Ye, and Y. Shi. 2012. 'Characterization of TLX expression in neural stem cells and progenitor cells in adult brains', *PLoS One*, 7: e43324.

Lois, C., J. M. Garcia-Verdugo, and A. Alvarez-Buylla. 1996. 'Chain migration of neuronal precursors', *Science*, 271: 978-81.

Lugert, S., O. Basak, P. Knuckles, U. Haussler, K. Fabel, M. Gotz, C. A. Haas, G. Kempermann, V. Taylor, and C. Giachino. 2010. 'Quiescent and active hippocampal neural stem cells with distinct morphologies respond selectively to physiological and pathological stimuli and aging', *Cell Stem Cell*, 6: 445-56.

Luo, J., X. Chen, Y. W. Pan, S. Lu, Z. Xia, and D. R. Storm. 2015. 'The type 3 adenylyl cyclase is required for the survival and maturation of newly generated granule cells in the olfactory bulb', *PLoS One*, 10: e0122057.

Luque-Molina, I., P. Khatri, U. Schmidt-Edelkraut, I. K. Simeonova, G. Holzl-Wenig, C. Mandl, and F. Ciccolini. 2017. 'Bone Morphogenetic Protein Promotes Lewis X Stage-Specific Embryonic Antigen 1 Expression Thereby Interfering with Neural Precursor and Stem Cell Proliferation', *Stem Cells*, 35: 2417-29.

Luque-Molina, I., Y. Shi, Y. Abdullah, S. Monaco, G. Holzl-Wenig, C. Mandl, and F. Ciccolini. 2019. 'The Orphan Nuclear Receptor TLX Represses Hes1 Expression, Thereby Affecting NOTCH Signaling and Lineage Progression in the Adult SEZ', *Stem Cell Reports*, 13: 132-46.

Malatesta, P., M. A. Hack, E. Hartfuss, H. Kettenmann, W. Klinkert, F. Kirchhoff, and M. Gotz. 2003. 'Neuronal or glial progeny: regional differences in radial glia fate', *Neuron*, 37: 751-64.

Merkle, F. T., Z. Mirzadeh, and A. Alvarez-Buylla. 2007. 'Mosaic organization of neural stem cells in the adult brain', *Science*, 317: 381-4.

Mich, J. K., R. A. Signer, D. Nakada, A. Pineda, R. J. Burgess, T. Y. Vue, J. E. Johnson, and S. J. Morrison. 2014. 'Prospective identification of functionally distinct stem cells and neurosphere-initiating cells in adult mouse forebrain', *Elife*, 3: e02669.

Ming, G. L., and H. Song. 2011. 'Adult neurogenesis in the mammalian brain: significant answers and significant questions', *Neuron*, 70: 687-702.

Mirzadeh, Z., F. T. Merkle, M. Soriano-Navarro, J. M. Garcia-Verdugo, and A. Alvarez-Buylla. 2008. 'Neural stem cells confer unique pinwheel architecture to the ventricular surface in neurogenic regions of the adult brain', *Cell Stem Cell*, 3: 265-78.

Misson, J. P., C. P. Austin, T. Takahashi, C. L. Cepko, and V. S. Caviness, Jr. 1991. 'The alignment of migrating neural cells in relation to the murine neopallial radial glial fiber system', *Cereb Cortex*, 1: 221-9.

Monaco, Sara, Katja Baur, Andrea Hellwig, Gabriele Hölzl-Wenig, Claudia Mandl, and Francesca Ciccolini. 2019. 'A Flow Cytometry-Based Approach for the Isolation and Characterization of Neural Stem Cell Primary Cilia', *Front Cell Neurosci*, 12.

Nam, H. S., and M. R. Capecchi. 2020. 'Lrig1 expression prospectively identifies stem cells in the ventricular-subventricular zone that are neurogenic throughout adult life', *Neural Dev*, 15: 3.

Nkomozepi, P., P. Mazengenya, and A. O. Ihunwo. 2019. 'Age-related changes in Ki-67 and DCX expression in the BALB/ c mouse (Mus Musculus) brain', *Int J Dev Neurosci*, 72: 36-47.

Obernier, K., and A. Alvarez-Buylla. 2019. 'Neural stem cells: origin, heterogeneity and regulation in the adult mammalian brain', *Development*, 146.

Obernier, K., A. Cebrian-Silla, M. Thomson, J. I. Parraguez, R. Anderson, C. Guinto, J. Rodas Rodriguez, J. M. Garcia-Verdugo, and A. Alvarez-Buylla. 2018. 'Adult Neurogenesis Is Sustained by Symmetric Self-Renewal and Differentiation', *Cell Stem Cell*, 22: 221-34 e8.

Obernier, K., I. Simeonova, T. Fila, C. Mandl, G. Holzl-Wenig, P. Monaghan-Nichols, and F. Ciccolini. 2011. 'Expression of Tlx in both stem cells and transit amplifying progenitors regulates stem cell activation and differentiation in the neonatal lateral subependymal zone', *Stem Cells*, 29: 1415-26.

Ortiz-Alvarez, G., M. Daclin, A. Shihavuddin, P. Lansade, A. Fortoul, M. Faucourt, S. Clavreul, M. E. Lalioti, S. Taraviras, S. Hippenmeyer, J. Livet, A. Meunier, A. Genovesio, and N. Spassky. 2019. 'Adult Neural Stem Cells and Multiciliated Ependymal Cells Share a Common Lineage Regulated by the Geminin Family Members', *Neuron*, 102: 159-72 e7.

Penisson, M., J. Ladewig, R. Belvindrah, and F. Francis. 2019. 'Genes and Mechanisms Involved in the Generation and Amplification of Basal Radial Glial Cells', *Front Cell Neurosci*, 13: 381.

Reynolds, B. A., and S. Weiss. 1992. 'Generation of neurons and astrocytes from isolated cells of the adult mammalian central nervous system', *Science*, 255: 1707-10.

Schindelin, J., I. Arganda-Carreras, E. Frise, V. Kaynig, M. Longair, T. Pietzsch, S. Preibisch, C. Rueden, S. Saalfeld, B. Schmid, J. Y. Tinevez, D. J. White, V. Hartenstein, K. Eliceiri, P. Tomancak, and A. Cardona. 2012. 'Fiji: an open-source platform for biological-image analysis', *Nat Methods*, 9: 676-82.

Scott, C. E., S. L. Wynn, A. Sesay, C. Cruz, M. Cheung, M. V. Gomez Gaviro, S. Booth, B. Gao, K. S. Cheah, R. Lovell-Badge, and J. Briscoe. 2010. 'SOX9 induces and maintains neural stem cells', *Nat Neurosci*, 13: 1181-9.

Seri, B., J. M. Garcia-Verdugo, B. S. McEwen, and A. Alvarez-Buylla. 2001. 'Astrocytes give rise to new neurons in the adult mammalian hippocampus', *J Neurosci*, 21: 7153-60.

Shen, Q., Y. Wang, E. Kokovay, G. Lin, S. M. Chuang, S. K. Goderie, B. Roysam, and S. Temple. 2008. 'Adult SVZ stem cells lie in a vascular niche: a quantitative analysis of niche cell-cell interactions', *Cell Stem Cell*, 3: 289-300.

Shingo, T., C. Gregg, E. Enwere, H. Fujikawa, R. Hassam, C. Geary, J. C. Cross, and S. Weiss. 2003. 'Pregnancy-stimulated neurogenesis in the adult female forebrain mediated by prolactin', *Science*, 299: 117-20.

Silva-Vargas, V., A. R. Maldonado-Soto, D. Mizrak, P. Codega, and F. Doetsch. 2016. 'Age-Dependent Niche Signals from the Choroid Plexus Regulate Adult Neural Stem Cells', *Cell Stem Cell*, 19: 643-52.

Steiner, B., F. Klempin, L. Wang, M. Kott, H. Kettenmann, and G. Kempermann. 2006. 'Type-2 cells as link between glial and neuronal lineage in adult hippocampal neurogenesis', *Glia*, 54: 805-14.

Stratton, J. A., P. Shah, S. Sinha, E. Crowther, and J. Biernaskie. 2019. 'A tale of two cousins: Ependymal cells, quiescent neural stem cells and potential mechanisms driving their functional divergence', *FEBS J*, 286: 3110-16.

Suh, H., A. Consiglio, J. Ray, T. Sawai, K. A. D'Amour, and F. H. Gage. 2007. 'In vivo fate analysis reveals the multipotent and self-renewal capacities of Sox2+ neural stem cells in the adult hippocampus', *Cell Stem Cell*, 1: 515-28.

Sun, W., A. Cornwell, J. Li, S. Peng, M. J. Osorio, N. Aalling, S. Wang, A. Benraiss, N. Lou, S. A. Goldman, and M. Nedergaard. 2017. 'SOX9 Is an Astrocyte-Specific Nuclear Marker in the Adult Brain Outside the Neurogenic Regions', *J Neurosci*, 37: 4493-507.

Tavazoie, M., L. Van der Veken, V. Silva-Vargas, M. Louissaint, L. Colonna, B. Zaidi, J. M. Garcia-Verdugo, and F. Doetsch. 2008. 'A specialized vascular niche for adult neural stem cells', *Cell Stem Cell*, 3: 279-88.

Than-Trong, E., S. Ortica-Gatti, S. Mella, C. Nepal, A. Alunni, and L. Bally-Cuif. 2018. 'Neural stem cell quiescence and stemness are molecularly distinct outputs of the Notch3 signalling cascade in the vertebrate adult brain', *Development*, 145.

Tramontin, A. D., J. M. Garcia-Verdugo, D. A. Lim, and A. Alvarez-Buylla. 2003. 'Postnatal development of radial glia and the ventricular zone (VZ): a continuum of the neural stem cell compartment', *Cereb Cortex*, 13: 580-7.

Waghmare, S. K., R. Bansal, J. Lee, Y. V. Zhang, D. J. McDermitt, and T. Tumbar. 2008. 'Quantitative proliferation dynamics and random chromosome segregation of hair follicle stem cells', *EMBO J*, 27: 1309-20.

Wang, L., M. Chopp, R. L. Zhang, L. Zhang, Y. Letourneau, Y. F. Feng, A. Jiang, D. C. Morris, and Z. G. Zhang. 2009. 'The Notch pathway mediates expansion of a progenitor pool and neuronal differentiation in adult neural progenitor cells after stroke', *Neuroscience*, 158: 1356-63.

Weber, T., V. Baier, R. Pauly, A. Sahay, M. Baur, E. Herrmann, F. Ciccolini, R. Hen, G. Kronenberg, and D. Bartsch. 2011. 'Inducible gene expression in GFAP+ progenitor cells of the SGZ and the dorsal wall of the SVZ-A novel tool to manipulate and trace adult neurogenesis', *Glia*, 59: 615-26.

Weigmann, A., D. Corbeil, A. Hellwig, and W. B. Huttner. 1997. 'Prominin, a novel microvilli-specific polytopic membrane protein of the apical surface of epithelial cells, is targeted to plasmalemmal protrusions of non-epithelial cells', *Proc Natl Acad Sci U S A*, 94: 12425-30.

Yuzwa, S. A., M. J. Borrett, B. T. Innes, A. Voronova, T. Ketela, D. R. Kaplan, G. D. Bader, and F. D. Miller. 2017. 'Developmental Emergence of Adult Neural Stem Cells as Revealed by Single-Cell Transcriptional Profiling', *Cell Rep*, 21: 3970-86.

Zeisel, A., H. Hochgerner, P. Lonnerberg, A. Johnsson, F. Memic, J. van der Zwan, M. Haring, E. Braun, L. E. Borm, G. La Manno, S. Codeluppi, A. Furlan, K. Lee, N. Skene, K. D. Harris, J. Hjerling-Leffler, E. Arenas, P. Ernfors, U. Marklund, and S. Linnarsson. 2018. 'Molecular Architecture of the Mouse Nervous System', *Cell*, 174: 999-1014 e22.

Zhuo, L., M. Theis, I. Alvarez-Maya, M. Brenner, K. Willecke, and A. Messing. 2001. 'hGFAP-cre transgenic mice for manipulation of glial and neuronal function in vivo', *Genesis*, 31: 85-94.

Figures

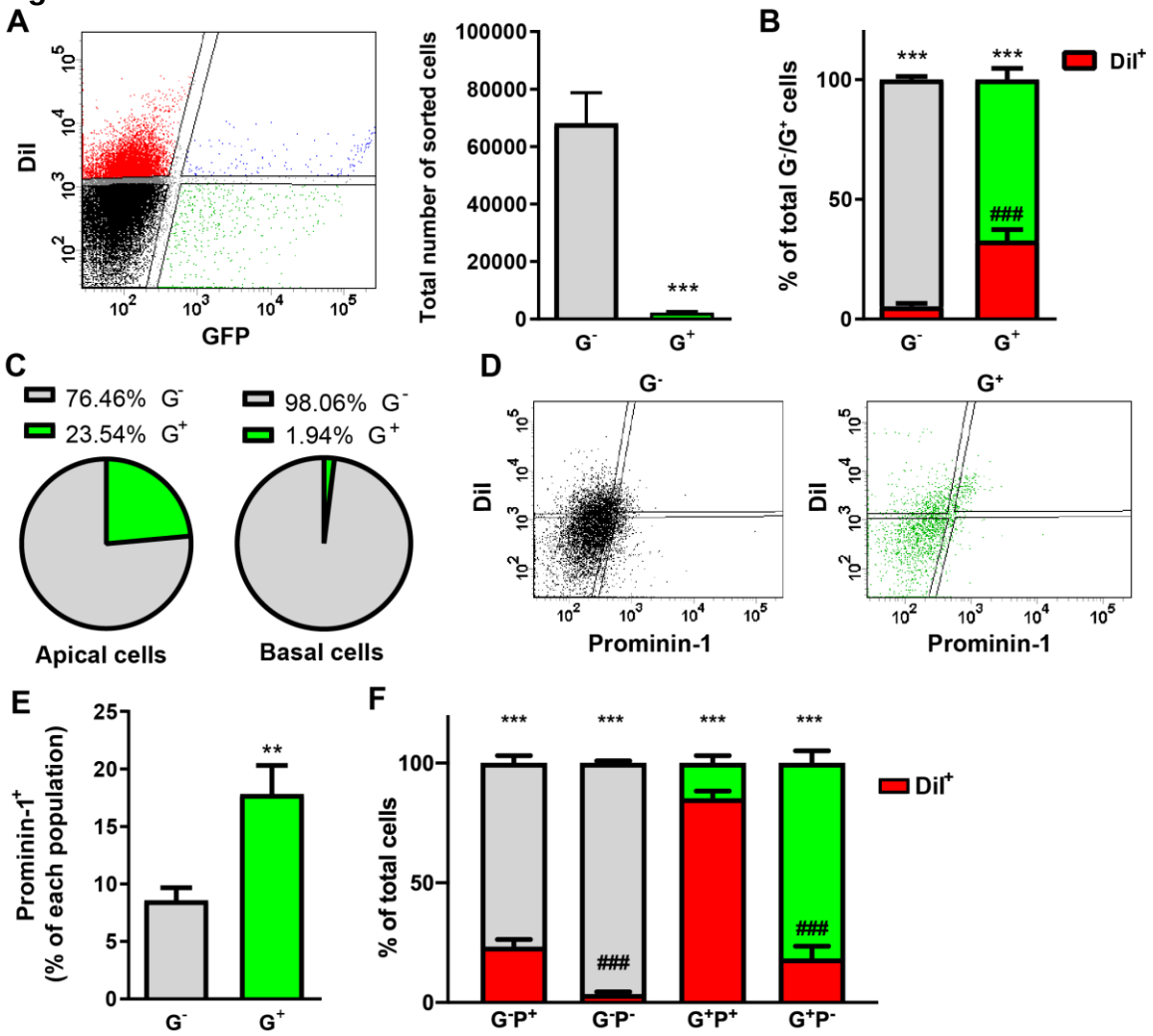

Figure 1: Most hGFAP-tagged cells do not display an apical membrane and Prominin-1 expression. (A) Representative FACS plot illustrating the distribution of dissociated V-SVZ cells according to their H2B-GFP (GFP) and DiI fluorescence (left panel). Quantitative analysis in the right panel shows the total number of V-SVZ cells expressing (G^+) or not (G^-) H2B-GFP. (B) Quantitative analysis of the percentage of DiI-labeled (DiI^+) apical cells within G^- and G^+ populations (C) and of the percentage of G^- and G^+ amongst total apical (DiI^+) and basal (DiI^-) V-SVZ cells. (D) Representative FACS plot of G^- cells (left panel) and G^+ cells (right panel) illustrating their distribution according to Prominin-1 and DiI fluorescence. (E) Quantification of the percentage of Prominin-1 immmunopositive cells in G^- and G^+ populations. (F) Quantitative analysis of the percentage of DiI^+ apical cells in each G^- and G^+ population sorted additionally on the basis of Prominin-1 (P) expression. Data is represented as mean ± SEM. N=29. * indicates significance between apical (DiI^+) and basal (DiI^-) cells within the same cell population and # indicates significance between G^- and G^+ in (B) and between G^-P^+ and G^-P^- or G^+P^+ and G^+P^- in (F). **p<0.01, ***/ ### p<0.001.

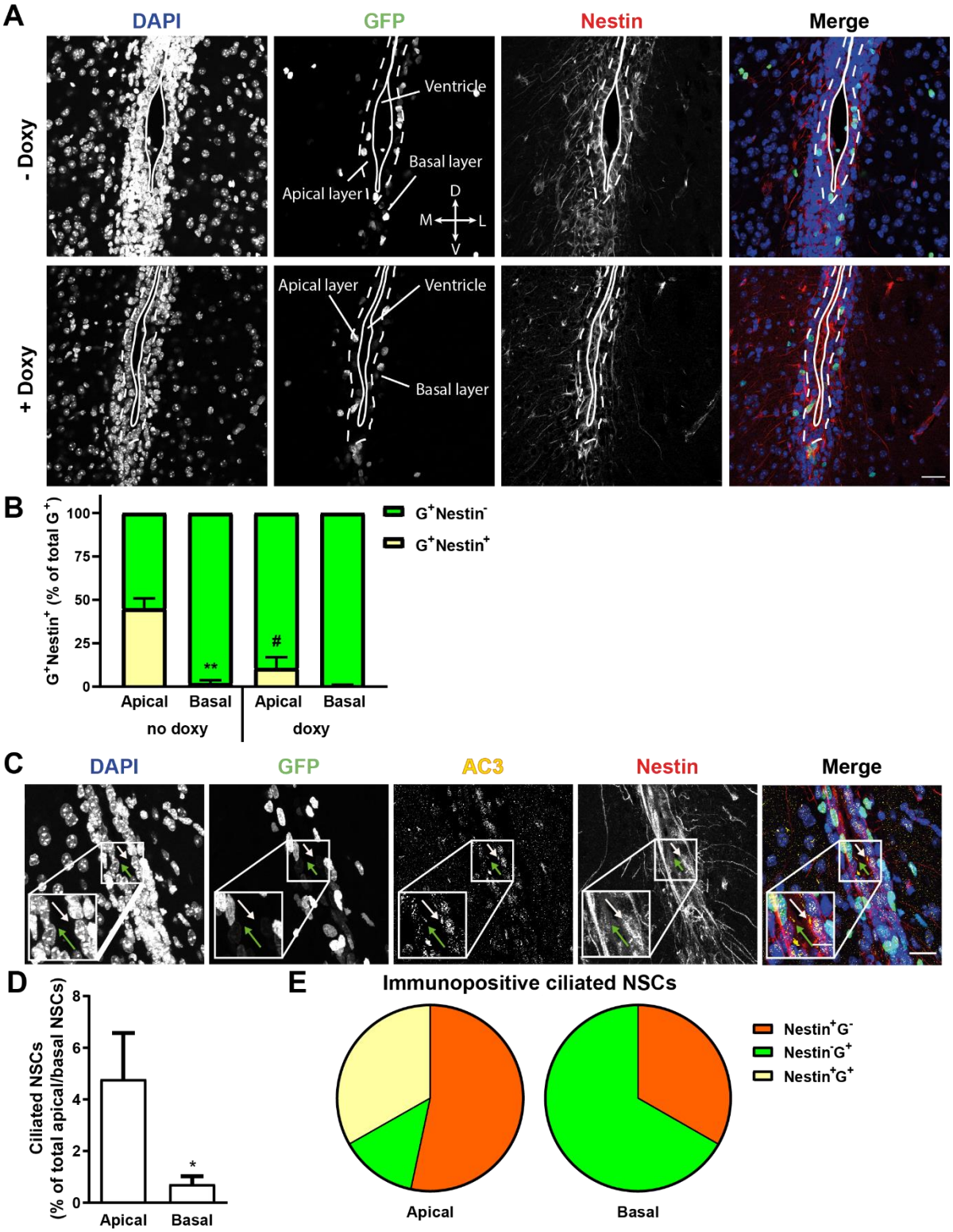

Figure 1: Basal hGFAP-tagged cells in the adult SVZ do not express Nestin and rarely extend primary cilia. (A) Confocal photomicrographs showing representative examples of coronal slices of the V-SVZ obtained from 8-weeks-old hGFAP;H2B-GFP mice treated with and without doxycycline (doxy) for 30 days as indicated. H2B-GFP (GFP) expression is shown in green, Nestin immunostaining in red and DAPI counterstaining of the nuclei in blue. Crossing arrows indicate slice directions: M = medial, D = dorsal, V = ventral, L = lateral. Continuous and dotted lines show the region

were the nuclei of apical cells were counted. (B) Quantification of marker expression in apical and basal cells in doxycycline-treated and untreated animals. N=3 (no doxy), N=4 (doxy) (C) Confocal photomicrographs illustrating a representative example of immunostaining of coronal slices of hGFAP;H2B-GFP mice not treated with doxycycline illustrating expression of H2B-GFP (GFP; green), Nestin (red) and AC3 (yellow) immunoreactivity and DAPI (blue) counterstaining of the nuclei. Arrows indicate Nestin-positive and GFP-positive cells with a primary cilium. (D) Quantification illustrate the percentage of ciliated apical and basal cells. (E) Pie charts represent antigenic characteristics of apical and basal ciliated cells. N=7. Scale bars = 30 µm; 10 µm for insert in (C). Bars represent mean ± SEM. * and # indicate significance: between apical and basal (*) and between doxycycline-treated and non-treated counterpart (#); */# $p<0.05$, **$p<0.01$.

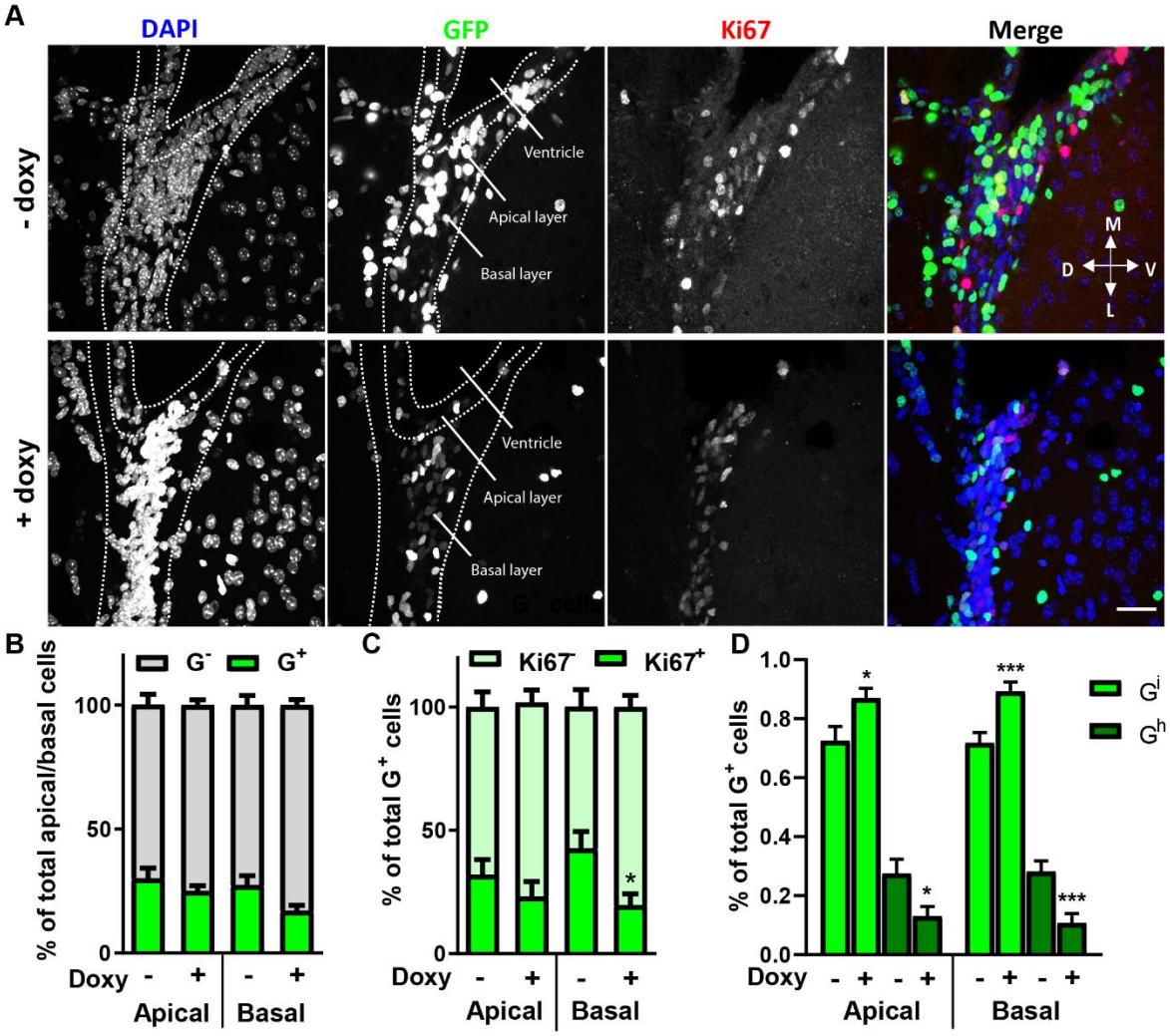

Figure 3: Apical and basal hGFAP-tagged cells both display NSC characteristics. (A) Repesentative confocal photomicrographs of coronal sections of the V-SVZ of 8W hGFAP;H2BGFP mice, which had been administered doxycycline (doxy) as indicated. Nuclear H2B-GFP (GFP) expression and Ki67 immunoreactivity are shown in green and red, respectively. DAPI counterstaining of the nuclei is blue. Scale bar= 30 µm. (B-D) Quantitative analyses of apical and basal cells expressing H2B-GFP (G^+) or not (G^-) (B), of Ki67 immunoreactivity in apical and basal G^+ cells (C), and of apical and basal cells expressing intermediate (G^i) or high (G^h) GFP levels with and without doxycycline (doxy) treatment (D). Data is represented as mean ± SEM N≥4. * indicates significance between doxycycline treated and nontreated specimens within apical or basal cell populations. * $p<0.05$, ***$p<0.001$.

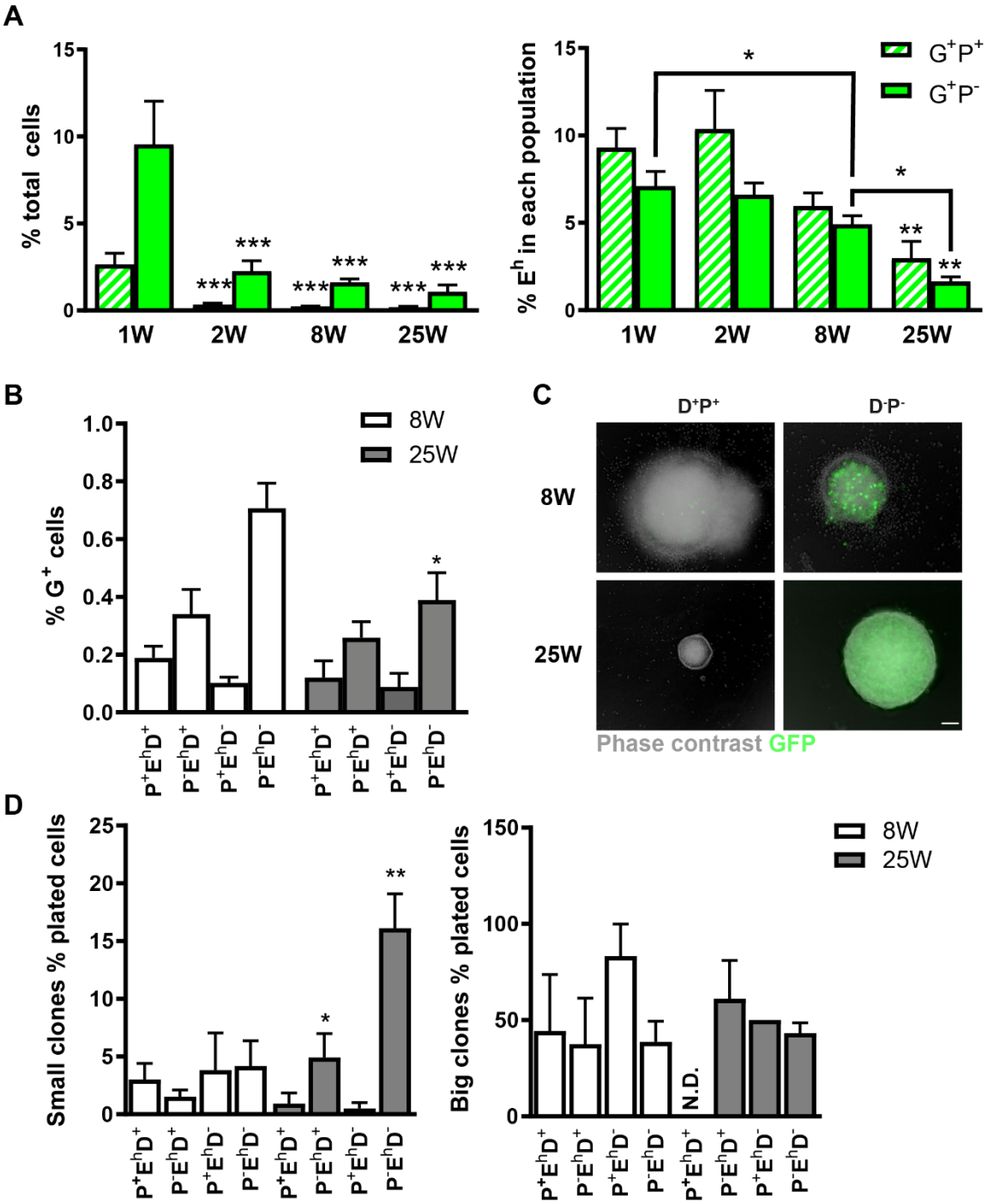

Figure 4: Basal NSCs represent the predominant stem cell population in the adult mouse brain. (A) Quantification of the flow cytometry analysis of the number of apical Prominin-1 immunopositive (G^+P^+) and basal Prominin-1 immunonegative (G^+P^-) cells (left panel) and of the percentage of activated cells expressing high levels of EGFR (E^h) in each population (right panel) at the various ages as indicated. * and # indicate significant difference from the respective 1W population, and 25W G^+P^- populations, ANOVA. (B) Quantitative analysis of the percentage of DiI-labelled apical (D^+) and basal (D^-) G^+ E^h cells expressing Prominin-1 (P) as indicated in the V-SVZ of 8- and 25-weeks-old animals. (C) Representative micrographs of clonal neurospheres generated from G^+E^h cells isolated at the indicated ages and displaying H2B-GFP (GFP), DiI labelling and Prominin-1 immunoreactivity. Scale bar=100 µm. (D)

Quantification of the percentage of the indicated subsets of G^+E^h cells generating small (left panel) and big (right panel) clones after sorting from 8W or 25W animals. Bars represent mean ± SEM. N≥4. * indicate in (A) significant difference from the corresponding 1W population (on top of bars) or between ages (lines) as indicated, in (B) and (D) from the respective population at 8 W. * $p<0.05$, ** $p<0.01$, *** $p<0.001$.

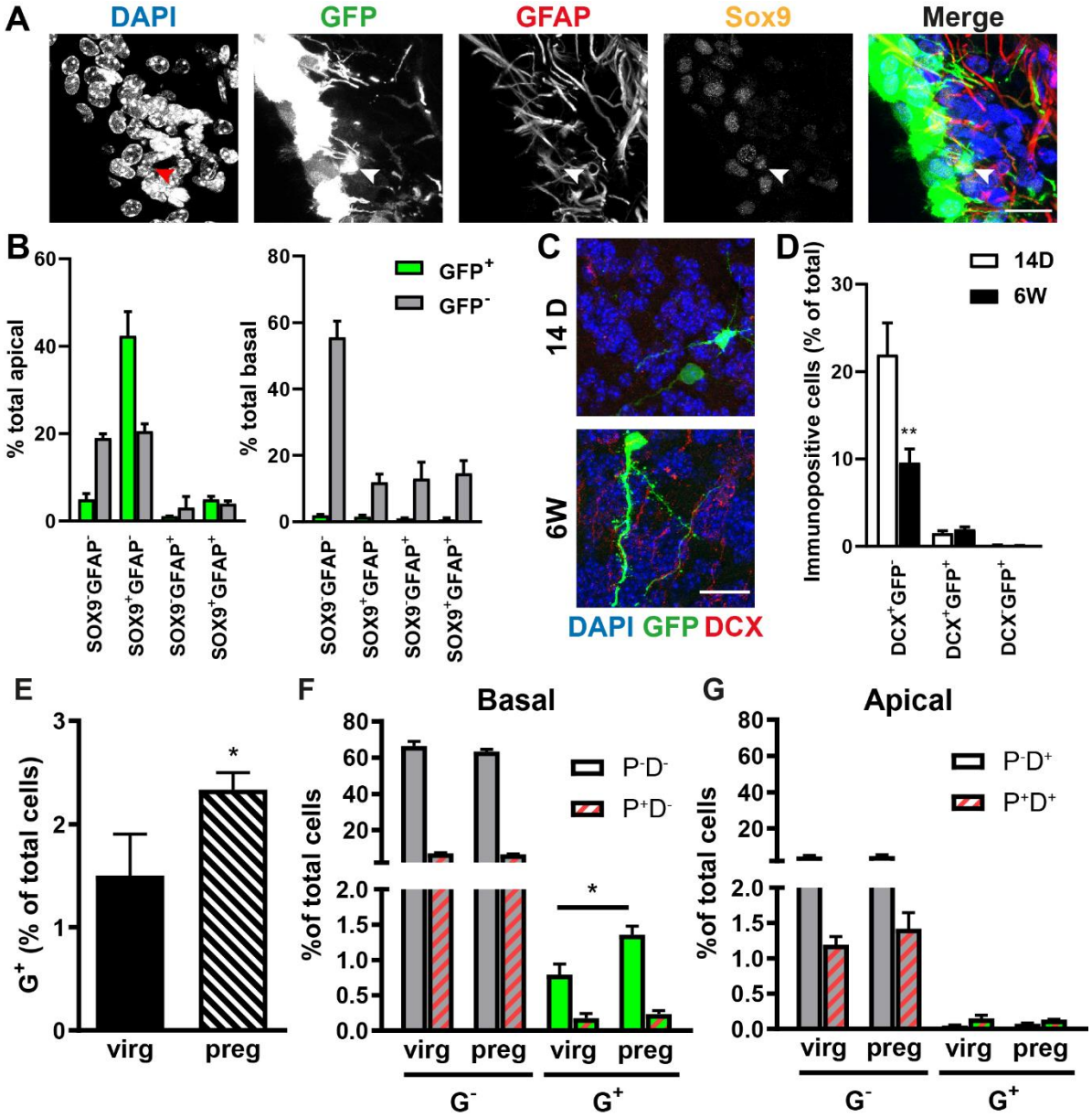

Figure 5: Apical NSCs give rise to few basal NSC-like cells in the SVZ and new OB interneurons. (A) Representative confocal photomicrographs of coronal sections of WT mice intraventricularly injected with AAV-GFP, and immunostained for GFAP and Sox9 at 14 days after injection. Scale bar = 30 µm. (B) Quantification of apical and basal GFP^+ and GFP^- cells expressing Sox9, GFAP or both. (C) Representative micrographs of the OB of AAV-GFP-injected animals, at 14 days (14D) and 6 weeks (6W) post injection. Scale bar = 20 µm. (D) Quantification of GFP^+ and DCX^+ cells in the OB, as percentage of total DAPI cells. (E) Percentage of G^+ cells counted by flow cytometry as % of total viable V-SVZ cells. (F, G) Expression of Prominin-1 (P^+/P^-) and DiI labelling (D^+/D^-) in G^+ and G^- cells isolated from virgin (Virg) and dames sacrificed immediately after giving birth (preg). Bars represent mean ± SEM, N≥3. * indicates significance: *p<0.05.

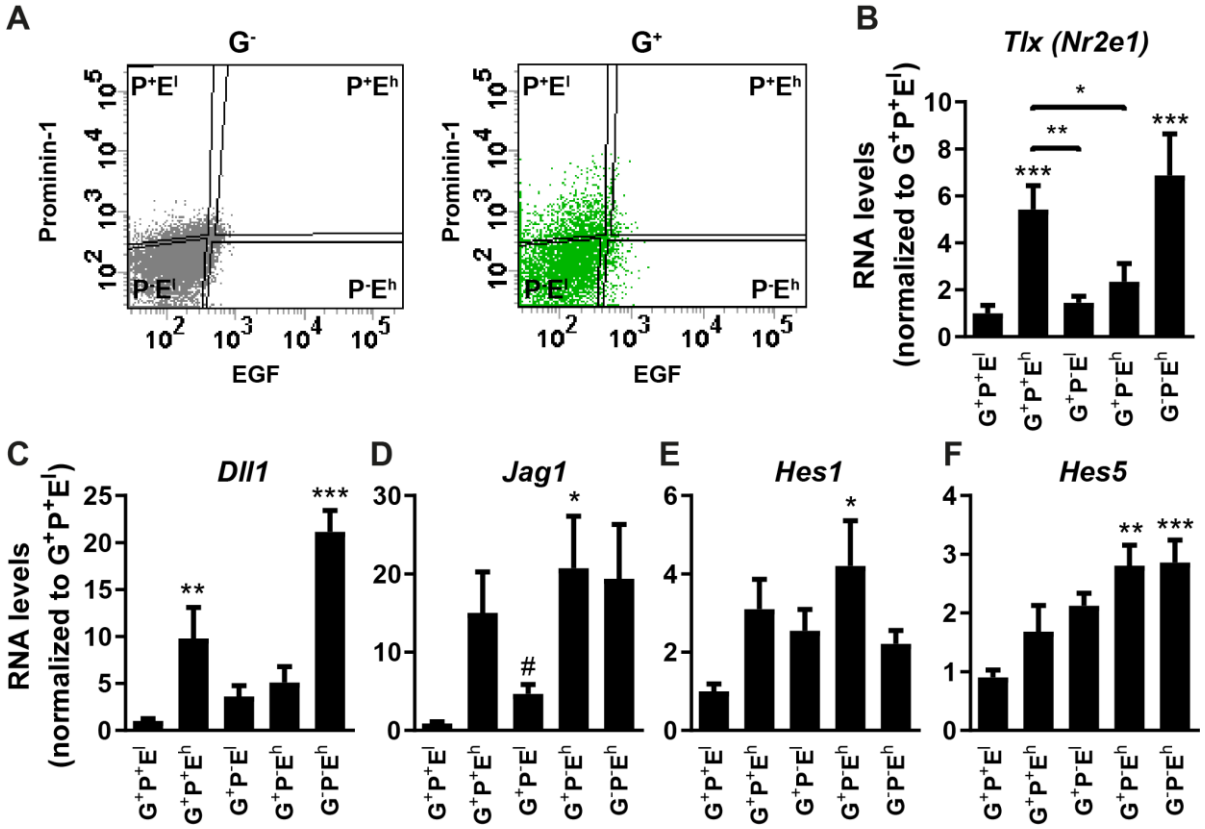

Figure 6: Expression of Notch signaling-related proteins in NSCs of the SVZ. (A) Representative FACS plots of G^- and G^+ cells sorted for EGFR and Prominin-1. (B-F) Fold change of mRNA levels for the indicated genes. Bars represent mean ± SEM, N≥4.*/# indicate significance to $G^+P^+E^l$ population or as indicated (lines), calculated by one-way ANOVA (*) or by student's t-test (#). */#p<0.05, **p<0.01, ***p<0.001.

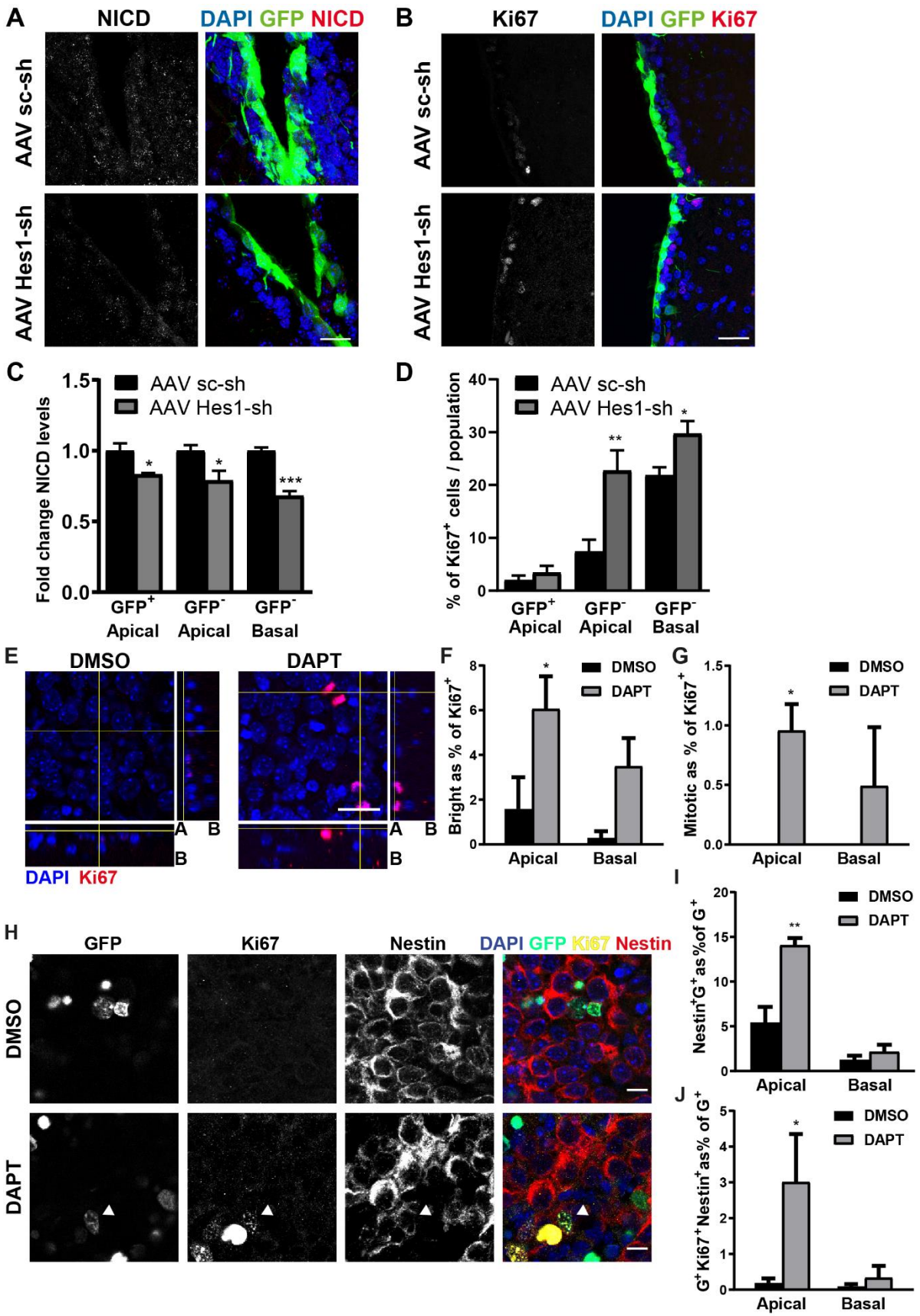

Figure 7: *In vivo* and *in vitro* interference with the Notch signaling pathway leads to increased proliferation of apical NSCs and intermediate progenitors. (A, B) Representative confocal photomicrographs the V-SVZs of mice injected with an AAV-expressing GFP and a shRNA against Hes1 (AAV Hes1-sh) or a scrambled sequence (AAV sc-sh) as a control. Coronal sections were stained with antibodies to either the

Notch intracellular domain (NICD, A) or Ki67 (B) to visualize actively cycling cells. DAPI was used for nuclear counterstain, scale bars = 100 µm. (C, D) Quantification of fold change in $NICD^+$ (C) or $Ki67^+$ cells (D). (E) Representative micrographs of the SVZ whole mounts which have been treated for 24 hours with DAPT or DMSO (control) and stained with Ki67 and DAPI. Scale bar = 20 µm. (F,G) Quantification of apical and basal bright $Ki67^+$ cycling cells (F) and cells undergoing mitosis (G). (H) Representative micrographs of whole mounts from hGFAP-H2BGFP mice treated with DMSO or DAPT, labelled for Ki67 and Nestin and counterstained with DAPI. Scale bars = 10 µm. (I,J) Quantification of cells positive for GFP, Nestin and Ki67 (I) or Nestin and GFP only (J), as percentage of total apical or basal G^+ cells. Bars represent mean ± SEM, N≥3. * indicates significance within each population. *p<0.05, **p<0.01, ***p<0.001.